EFFECTIVE TEMPERATURES AND LUMINOSITIES OF VERY HOT O-TYPE SUBDWARFS[1]

D. Schönberner[2] and J. S. Drilling[2]

Louisiana State University Observatory

ABSTRACT

We observed 12 very hot O-type subdwarfs with the IUE-satellite in the low dispersion mode. We derived temperatures from the slopes of the UV-continua and estimated distances from the color excesses. Most of them are hotter than 60,000 K, i.e. they are the hottest known subdwarfs. From their spectral appearance and location in a H.R.-diagram they form a rather inhomogeneous group. Three of them turned out to be central stars or nearly central stars, and four are definitely near the white dwarf stage. The surface helium to hydrogen ratio varies from about normal to the extreme case. Most of them appear to be post EHB objects of 0.5 M_o with a helium burning shell as their energy source, and their peculiar helium-to-hydrogen ratios are most likely the result of diffusion and convective mixing in surface layers.

Subject Headings: stars: O-type subdwarfs - stars: white dwarfs - stars: evolution - stars: interiors - nebulae: planetary

[1]Contributions of the Louisiana State University Observatory No. 000.

[2]Guest observer with the International Ultraviolet Explorer Satellite which is sponsored and operated by the National Aeronautics and Space Administration, the Science and Engineering Research Council of the United Kingdom, and the European Space Agency.

I. INTRODUCTION

The subluminous O stars are of great importance to our understanding of the late phases of stellar evolution, as they appear, along with the central stars of planetary nebulae, to be the immediate progenitors of white dwarfs. Greenstein and Sargent (1974) gave a first detailed examination of sdO's in their investigation of faint blue halo stars. These stars bridge a considerable range in luminosity from several times 10^3 L_o (some central stars are classified as sdO) down to ~ 10 L_o. From their spectral appearance, they form a very inhomogeneous group: some are helium rich, others helium poor (Hunger et al. 1981). Some are members of binary systems (e.g. HD 49798, Kudritzki and Simon 1978), and their history and peculiarity can be explained by binary evolution with mass exchange. Most of them, however, appear to be single, and their origin is still speculative. We can only state that most of them are highly evolved, low-mass stars ($M < 0.6\ M_o$) which were unable to climb the giant branch a second time.

A very important question posed by Greenstein (1980) is how hot an O-type subdwarf can be. He studied 7 sdO's by means of the IUE-statellite and found an upper temperature limit of ~ 60,000 K. This is in agreement with a NLTE-study of a different set of 11 sdO's performed by Hunger et al. (1981). This temperature limit, if real, will be an important constraint for any explanation of their evolutionary status.

We present IUE-observations of 12 newly-detected, relatively bright O-type subdwarfs ($V < 13$), which are the result of a complete survey of non-emission OB+ stars in the area $b = \pm 30$, $l = \pm 60^o$ done by Drilling (1983). These IUE observations enabled us to derive reliable temperatures by comparing the observed fluxes with those from model atmospheres (Sec. II). Since our objects are confined to the galactic plane, we can estimate their distances

from the strength of the 2200 A feature. This gives us their loci in a H.R.-diagram (Sec. III), which we shall discuss in terms of stellar interior calculations.

II. OBSERVATIONS AND REDUCTIONS

We observed the 12 subluminous O stars which have recently been detected by Drilling (1983) in the large aperture, low resolution mode of the IUE satellite. The objects and the image numbers are given in Table 1. We got well exposed images in both cameras, and we employed the absolute calibration of Bohlin and Holm (1980) to get absolute fluxes. We determined the color excess in the usual way by nullifying the interstellar absorption feature at 2200 A with Seaton's (1979) mean reddening law. In all cases, the color excess is small, the largest value being 0.25 magnitudes. Thus we do not expect large errors to be caused by the application of a mean reddening law. The photometric color excesses are given in parentheses in Table 1 for those objects with available UBV photometry (Drilling 1983), under the assumption that $(B-V)_0 = -0.35$. The average difference in the color excesses derived by the two methods is +0.005 (IUE minus photometric), indicating that there are no significant systematic errors.

The dereddened spectrograms are displayed in Fig. 1, where they are arranged by decreasing gradient of the UV-flux (see below). They reveal a wide variety of spectral appearances because of the different strengths of the NV, SIV, CIV, HeII and L_α lines. Some objects show the He II $3 \rightarrow \infty$ series (the limit is at 2050 A) very clearly. SiIV is weak in all cases. Three objects show evidence for mass loss: LSS 2018 and LSE 125 have blueward displaced NV absorptions, and in LSE 259, P-Cygni profiles of NV and CIV are

present. In the latter case, the NV absorption is the strongest of all 12 objects. The blueward shifts correspond to wind velocities of 1900 to 2400 km/s. Some spectra appear to be very similar to those of the faint central stars observed by Kaler and Feibelmann (1983). We want to emphasize that even these very hot stars show important line-blocking, mostly shortward of 1600 A. The importance of UV line blocking (and blanketing as well) for hot stars has already been pointed out by Bruhweiler, Kondo and McCluskey (1981). We have a high dispersion study of our brightest sdO's underway, and as a preliminary result we can report that most of the line blocking is caused by photospheric absorption lines of FeIV and FeV.

Because a reliable temperature determination was our main goal, we employed a new method which we shall now describe in detail. It has already been stated in the literature (e.g., Greenstein 1980) that the photometric accuracy of the IUE-satellite is sufficient to discriminate an object with 100,000 K or more from cooler ones. Normally, one tries to match the visual flux (e.g., at V) and the UV-flux by a black body or a model atmosphere with the appropriate temperature. For hot objects, this method is not recommended, because the change in the flux gradient caused by a small error in the color excess will cause a large error in the temperature. Instead, we measured the ratio of the total fluxes from the two cameras, i.e.

$$R = \int_{1240}^{1945} F_\lambda \, d\lambda \Big/ \int_{1945}^{3120} F_\lambda \, d\lambda$$

The integration boundaries are somewhat arbitrary. We chose them to cover most of the IUE range of sensitivity while avoiding strong interstellar and/or geocoronal L_α-features. To get a reasonably accurate flux, a broadband integration is especially necessary for the relatively noisy LWR camera.

It turns out that R is nearly independent of the reddening. For instance, a change in the color excess of 0.1 magnitudes corresponds to only $\frac{\Delta R}{R} = 0.04$! The reason is the peculiar wavelength dependence of the interstellar absorption curve: the 2200 A bump in the LWR wavelength region nearly compensates for the absorption between 1200 and 1800 A. Thus a small error in the color excess does not significantly influence R, the error of which we conservatively estimate to be within 3% for well exposed images. More serious might be any systematic error arising from differences in the photometric accuracy of the two cameras. We do not know this error, but we want to state here that the two cameras give good agreement in the overlapping wavelength region. In principle it is straightforward to calibrate R as a function of the effective temperature by means of model atmospheres. In practice, however, one encounters two difficulties: (1) we have line blocking which is not included in the model atmospheres, and (2) the UV flux gradient depends on the He/H ratio as well as on the temperature.

We proceeded in the following way: First we fit each (dereddened) spectrogram with a black body flux distribution in such a manner that it appeared as the upper boundary of the observed flux. Fig. 2 shows the measured R plotted against the temperatures of these black bodies, with a typical error also shown. The errors in the temperatures (~20%) arise primarily from the uncertainty in the color excesses. Also plotted is the relation given by Planck's law. Our objects are below the black body curve because the stellar lines depress the flux primarily in the SWP region. The scatter around a straight line is only moderate, at most ±0.04 in log T_{eff} or ± 10% in T_{eff}. This fact is very satisfying because the fitting process depends on the assumed color excess and can therefore be an important source of error. The good correlation between R and T_{BB} proves that we found consistency between a

reddening independent quantity (R) and the reddening dependent continuum slope (which actually defines the temperature), and that we can measure (color) temperature differences within a 10% accuracy by using the parameter R as a temperature indicator. There is, however, one exception: LSE 234 is too hot for its R value. This is caused by an excessively large amount of blocking between 1600 and 2000 A, which reduces the SWP contribution to R for LSE 234. It would be desirable to confirm this observed flux depression with additional observations. Two objects, LSS 1362 and LSE 21, have flux gradients which are equal to or in excess of the theoretical limit (a black body of infinite temperature gives R = 3.78). It is unlikely that a different color excess or even a different reddening law would resolve this problem, since both stars are only moderately reddened (0.18 and 0.19 magnitudes, respectively). Even without any correction for interstellar reddening, the R values are larger than 3.5 in both cases. Clearly, both of these stars are candidates for the hottest known stars, with effective temperatures certainly in excess of 100,000 K! We shall come back to this problem later.

As a next step, we looked for a model atmosphere with the same flux gradient between 1200 and 3100 A as the fitting black body (by interpolating in our model grid), and considered the effective temperature of this model to be that of our star. To proceed in this way, we computed a grid of high-temperature (40,000-300,000 K), high gravity (log g = 4.5 - 8.0) LTE atmospheres with pure hydrogen-helium compositions in various mixtures [n(He)/n(H) = 0.1, 1.0 and ∞]. The UV flux gradient is only weakly dependent on gravity, but is highly dependent on composition. For a pure helium composition this gradient is lower than that of a hydrogen dominated atmosphere of the same temperature, and is nearly the same as that of a black body with the same temperature. The difference between the two extreme compositions is largest around 60,000 K where a helium rich atmosphere

yields a 25% higher temperature than one with a normal composition. For this very reason it is not necessary to use more sophisticated model atmospheres with the inclusion of metallic opacities or even NLTE-effects, which will only change the gradient between 1200 and 3100 Å by a negligible amount. Needless to say, the amount of line blocking between 228 and 911 Å and its consequences on the temperature stratification are completely unknown.

We tested our method in the following way: we chose 4 hot standard stars which have already been observed with the IUE satellite and which have reasonably well known effective temperatures and compositions. These objects and the pertinent data are listed in Table 2. Column 5 of Table 2 gives the measured R, and column 4 the temperature of a black body which best matches the flux between 1200 and 3200 Å of our model atmosphere corresponding to the published temperature, gravity and composition. These four objects are also displayed in Fig. 2, and their positions agree very well with our empirical R, T_{BB} correlation, though a slightly systematic difference of $\Delta \log T_{BB} \simeq 0.05$ seems to be present at high temperatures.

Please note that NGC 7293 has R well above the limit of infinite temperature. Since this nearby star is practically unreddened - $E_{B-V} = 0.012$ according to Bohlin et al. (1982) - we believe that this is due to an error in the photometric calibration of IUE below $\lambda \sim 1500$ Å. Fig. 1 of Bohlin et al. (1982) clearly shows excessive fluxes of up to 10% at short wavelengths when compared to the model atmosphere prediction, and we suggest a careful inspection of the SWP photometric calibration using very hot stars. This calibration error can well explain the small systematic difference between our R, T_{BB} correlation and that of the four standard stars, and also the existence of UV flux gradients much steeper than those of a black body of infinite temperature.

We have collected the results for our sdO's in Table 3, which gives the measured flux ratios (R), the effective temperatures for two compositions, and the black-body temperatures for comparison. Since LSE 21 and LSS 1362 have nearly the same R as NGC 7293 we adopt $T_{BB} \approx 170{,}000$ K for these two stars. Taking the cooler set of temperatures, we see that at least one half of our objects have effective temperatures in excess of 60,000 K, the upper limit quoted by Greenstein (1980). Because UBV photometry is available for most of our objects (Drilling 1983), we are able to check the compatibility of our IUE-based results with ground-based measurements. In all cases we found satisfactory agreement. An illustrative example is shown in Fig. 3, where IUE and UBV data of LSS 2018 are compared with 80,000 K and 100,000 K models of normal composition. The 100,000 K model seems to fit the observations better, but our method, which uses only the IUE data, favors a temperature nearer to 80,000 K (see Table 3). Remember that a 1% error in the color excess corresponds to an 7% change in the flux at 1200 A relative to that at 5500 A, which is comparable to the flux difference between the two models. This demonstrates clearly that the use of a long baseline can be unprofitable in cases where the wavelength dependence of the stellar flux is approaching the Rayleigh-Jeans limit and the color excess competes with the temperature in determining the stellar flux gradient. In addition, we have to be aware of the possibility of systematic differences between the IUE calibration and that of the UBV system. For the latter, we used the calibration recommended by Hayes (1979).

An additional systematic error in our temperature determination is caused by the unknown surface abundances. We can reduce this uncertainty if we know something about the individual helium-to-hydrogen ratios. Fortunately, only rough estimates are necessary: for $n(He)/n(H) \gtrsim 1$, the flux distribution

between 1200 and 3000 A is nearly the same as it is for n(He)/n(H) = ∞, and for n(He)/n(H) < 0.3, models with the standard helium content are adequate. We estimated the helium abundance by comparing visible spectra of 40 A/mm dispersion with those of stars of known helium abundance (see Drilling 1983). These estimates together with the finally adopted temperatures are also given in Table 3. These are the temperatures of the models with n(He)/n(H) = 1 in cases where helium enrichment is indicated, and are otherwise the temperatures of models with n(He)/n(H) = 0.1. Please note that two of the coolest of our objects, LSE 259 and LSIV +10°9, are probably extremely helium- rich because they have very weak L_α-absorptions (Fig. 1). This would be consistent with the appearance of the visible spectrum (Drilling 1983). These two stars have temperatures of about 60,000 K and are a little bit hotter than the hottest object analyzed by Hunger et al. (1981), LSS 630 with a temperature of 55,000 K. LSIV 10°9, a higher gravity object, is the only member of our ensemble which shows He I-lines at moderate dispersion (40 A/mm), whereas these lines are clearly visible in LSS 630 and cooler objects (Hunger et al. 1981, Fig. 1a).

III. THE H.R.-DIAGRAM AND THE EVOLUTION OF SDO'S

Since our program stars are confined to the galactic plane and have measurable color excesses, we tried to estimate their distances. We used the graphs of FitzGerald (1968), Lucke (1978), Nandy et al. (1978), and in some cases Perry and Johnston (1982), and Table 4 shows the results. Visual magnitudes are from Drilling (1983). In most cases we found reasonable agreement between the different authors. In only two cases were we unable to determine a consistent distance: LSS 1362 and LSE 21. From Lucke and Nandy et al. distances of ~ 500 pc to > 1000 pc follow in both cases, but according to

Fig. 3 of FitzGerald, the distances can be as low as 50-100 pc, making them as faint as $M_V \sim 7$ or 8. These low luminosities are in accordance with their spectral appearance (Drilling 1983), and we therefore adopt them in Table 4. The (visual) luminosities shown in Table 4 cover a wide range, namely from ~ 1.5 down to ~ 8 magnitudes, in agreement with Greenstein and Sargent's (1974) finding. For the convenience of the reader, we have also derived bolometric luminosities by simply applying bolometric corrections (see below) to M_V. Our results for LSII $+18^{0}9$ and LSIV $+10^{0}9$ agree well with those of Walker (1981) who found $M_V \sim 7$ and $M_V > 3.2$, respectively.

The H.R.-diagram is shown in Fig. 4 in the form best for our purposes, M_V vs. log T_{eff}. The use of the visual instead of bolometric luminosity has the advantage of being independent of the effective temperature and its errors, i.e., only the distance errors enter into the ordinate. The interstellar absorption is small ($A_V < 0.6$) and cannot cause serious errors in M_V. This kind of diagram was also preferred by Greenstein and Sargent (1974). Evolution with constant luminosity proceeds on a nearly diagonal line. For better orientation, we also give the positions of the helium main sequence according to Paczynski (1971) and the low temperature borderline of the region where central stars of planetary nebulae are supposed to appear. This borderline was estimated from the temporal evolution of post-AGB models, thereby assuming a mean PN-lifetime of 40,000 yrs (Schönberner 1981, 1983). The (theoretical) evolutionary paths of central stars with 0.565 $M_\odot$ and 0.644 $M_\odot$ are also taken from (Schönberner 1979, 1983).

First we wish to repeat here that our objects are hotter than any other sdO's so far analyzed, i.e., 60,000 K or hotter. They occupy the area between the hot central stars and the He-main sequence. Two of them (LSS 2018 and LSE 125), with apparently normal compositions, are in the central star region.

Their high luminosities (>10^3 L_o, see Table 4) are consistent with the indications of mass loss found in their UV-spectra (Sec. III). Inspection of red ESO-survey plates (Drilling 1983) has revealed that both objects indeed have faint nebulosities around them (DS 1 and DS 2) with diameters of 180", corresponding to R_N = 0.48 and 0.26 pc, respectively, if we apply the distances of Table 4. According to their galactic coordinates, the Perek/Kohoutek designations would be DS 1 = 283 +9.1 and DS 2 = 336 +12.1. DS 1 was already suspected to be a planetary nebula: ESO-215-04 (Holmberg et al. 1978). The two nebulae can be considered to be members of the local ensemble, because their distances projected onto the plane are smaller than ~ 1000 pc.

We can use these PN to make a consistency check: using the (M_V, log t_{exp})-diagram given by Schönberner (1981, Fig. 7), and assuming a nebular expansion velocity of 20 km/s, we find T_{eff} ~ 70,000 K and M ~ 0.56 M_o for the nucleus of DS 1 (i.e., for LSS 2018), and T_{eff} ~ 105,000 K and M ~ 0.57 M for the nucleus of DS 2 (LSE 125), in excellent agreement with their positions in Fig. 4. LSIV -12^o1, also with normal composition, is placed near the luminosity limit for central stars. As a nebula is not detectable, we interpret LSII -12^o1 as a low-mass (M < 0.55 M_o), post-AGB object, whose age exceeded that of the accompanying nebula (Schönberner 1983).

LSE 44 and LSII 18^o9 are very faint, obviously entering the white dwarf cooling sequence at the lower mass side ($M/M_o \lesssim 0.55$). They will eventually become white dwarfs of spectral type DA. Four objects of intermediate luminosity are helium rich or even extremely helium rich and apparently a continuation to higher temperatures of the corresponding helium rich objects of Hunger et al. (1981). LSS 1362 and LSE 21 are very hot and most likely also very faint. Their position in Fig. 4 is somewhat uncertain, but it is obvious that they have higher masses (M > 0.6 M_o), and that they are in the transition

from a central star to a white dwarf. We were unable to detect any nebulosity around them.

We included also in Fig. 4 the objects analyzed by Hunger et al. (1981) and the sdB-ensemble of Heber et al. 1983 (some of these sdB are in fact sdOB). In order to convert their light-to-mass ratios into visual luminosities, we assumed a mass of 0.5 M_0 and the bolometric corrections given by Schönberner (1981). Most of these objects are on or even above the helium main sequence, whereas ours are below and may therefore represent the missing evolutionary link between the cooler objects (including the sdB's) and the final white dwarf stage. If so, the separation into groups with different atmospheric compositions (sdB, sdOB, and sdO) has to be due to surface effects, i.e., gravitational settling and convective mixing. The idea of gravitational settling and convective mixing was first introduced by Greenstein and Sargent (1974) and later discussed again by Hunger and Kudritzki (1981).

In the sdB-region, the helium convection zone is well below the atmospheric layers, and gravitational settling can deplete helium in a quiet atmosphere within only 5.10^3 yrs (Michaud et al. 1983). At $T_{eff} \simeq 10^{4.6}$ K, the helium convection reaches the surface ($\tau = 1$), and the helium is brought back to visible layers. Above $T_{eff} \simeq 10^{4.8}$ K, the convection turns off completely, so that gravitational separation of hydrogen and helium will work again (Winget and Cabot 1980, Wesemael et al. 1982). The observations seem to support this scheme: most helium-rich objects are confined between log $T_{eff} \simeq 4.8$ and $\simeq 4.6$ (Fig. 4), and in the later evolutionary phases, helium depletion is again indicated (LSE 234, LSE 44, LSII $+18^{o}9$).

Let us now consider objects on the extended horizontal branch (EHB), i.e., B-type subdwarfs, as the progenitors of O-type subdwarfs. We do not want to repeat here the difficulties which are associated with their origin. The

reader is referred to the discussions in Sweigart, Mengel and Demarque (1974), Baschek and Norris (1975) and Baschek et al. (1982). EHB-stars have $M \simeq 0.5\ M_\odot$ and a helium core of nearly the same mass: $q = M_{core}/M_* \geq 0.95$ (models with larger envelope masses are cooler and will evolve to lower temperatures according to Sweigert and Gross, 1976). The temperatures of such models depend sensitively on the envelope mass, and their loci are indicated in Fig. 4 for $M_c = 0.5\ M_\odot$, and different q. The models with q = 0.999 and q = 0.98 are from Caloi (1972), and that with q = 0.95 is from Sweigart and Gross (1976). These models have normal helium-to-hydrogen ratios in their envelopes; models with helium enriched envelopes would be placed nearer the helium main sequence. The hydrogen burning shell does not exist in practice (L_H is about 1% of the stellar luminosity), and these models will evolve like a pure helium star of $0.5\ M_\odot$, but somewhat shifted to lower effective temperatures. The evolution of a $0.5\ M_\odot$ pure helium star (Paczynski 1971), also shown in Fig. 4, is to be considered as an extreme, limiting case, as most observed stars are not completely hydrogen- depleted. The (estimated) track of a $0.5\ M_\odot$ star with a tiny hydrogen-rich envelope (i.e., q = 0.98) is indicated in Fig. 4 by a dashed line. After $\sim 10^8$ yrs helium ignites in the shell, and the model will leave the sdB region and enter first the sdOB, then the sdO region, as the computations of Paczyinski (1971) suggest. The following evolution from central helium exhaustion to a pre-white dwarf configuration lasts only about 2.10^7 yrs.

Thus this evolutionary scheme does not only connect sdB- and sdO-stars with the white dwarf region, but also predicts a much greater space density of sdB's than sdO's, a result which agrees at least qualitatively with the recent ultraviolet survey of Carnochan and Wilson (1983). All sdB's in Fig. 4 are located a little bit above the zero-age EHB, indicating that they are in an

advanced stage of central helium burning if we assume $M_* = 0.5\ M_\odot$ and $q \gtrsim 0.98$. According to Fig. 4, sdOB- and sdO-stars then represent the following phases of helium burning in a shell surrounding a growing, inert C/O-core, and the loci of some of them near the helium main sequence is purely accidental. In fact, if these were central helium burning objects, they would have to have masses of up to 1 $M_\odot$, which appears to be unrealistic.

Presently, two ways are thinkable to explain the observed overabundance of helium in the atmospheres of sdO-stars: First, let us assume that these objects began their EHB-evolution with a helium-enriched envelope as a result of a violent helium core flash (see discussion of Hunger and Kudritzki 1981). Helium will settle gravitationally during the central helium burning phase (sdB-region), but in the following sdO-phase helium convection will restore the original helium rich surface composition. The second way has been proposed by Winget and Cabot (1980) and Wesemael *et al.* (1982). Their envelope calculations demonstrate that helium convection is able to enrich the atmosphere with helium if less than $\sim 10^{-10}\ M_\odot$ of hydrogen-rich matter is floating above the pure helium layers. In this case we do not need a helium rich envelope to start with on the EHB. However, we cannot explain how such a stratified envelope developed. A possibility might be the combined action of mass loss and diffusion . Also, Wesemael *et al.* (1982) did not compute changes of the surface abundances. Thus a quantitative comparison between theoretical and observed abundances is presently impossible.

In principle, the CNO abundance distribution can answer the question of whether the helium which has been brought to the surface is the result of CNO-cycling (Case 2) or not (Case 1). The sdO's for which a reliable determination of the carbon and nitrogen abundances is available indicate that indeed CNO-cycled matter has been mixed to the surface. We have to warn, however, that

diffusion also affects the CNO-elemental distribution. We urgently need evolutionary calculations of EHB-stars which consider diffusion and convective mixing in the envelope, and mass loss as well.

Some objects in Fig. 4 have relatively high luminosities (and probably $M > 0.5\ M_o$), and cannot be reached by evolving EHB-models. We therefore believe that they represent a different evolutionary stage. They certainly have a hydrogen burning shell surrounding the helium burning core, which contributes significantly to their luminosity. They are probably descendents from the first giant branch. It is worth mentioning here a peculiar star which may have some connection to these higher mass subdwarfs: the pulsating star BD $+13^o3224$. This object is extremely helium rich, $n(He)/n(H) = 99$, and its mass and luminosity are known: $M = 0.9^{+0.5}_{-0.3}\ M_o$, $L = 10^{3.1\pm0.2}\ L_o$ (Hill et al. 1981). It has a decreasing pulsational period which indicates evolution towards the sdO-region, as indicated in Fig. 4. From the mass, luminosity, and composition it is clear that BD $+13^o3224$ is contracting to the helium main sequence, where helium will be ignited in its core. During the core helium-burning phase, BD $+13^o3224$ will appear as an extremely helium rich sdO.

ACKNOWLEDGEMENTS:

This research was supported in part by the National Aeronautics and Space Administration (Grant No. NAG 5-71), the National Science Foundation (Grant No. AST 8018766), and the Air Force Office of Scientific Research (Grant No. 82-0192). One of us (DS) also wishes to thank the Deutsche Forschungsgemeischaft for a travel grant. Our special thanks to N. P. Harris who did an excellent job on drawing the figures, and L. Gauthier who typed this manuscript with great patience.

REFERENCES

Auer, L. H., and Shipman, H. L. 1977, Ap. J. (Letters), 211, L103.

Baschek, B., and Norris, J. 1975, Ap. J. 199, 694.

Baschek, B., Kudritzki, R. P., Scholz, M., and Simon, K. P. 1982, Astr. and Ap., 108, 387.

Bohlin, R., and Holm, A. 1980, NASA IUE Newsletter No. 10, p. 37.

Bohlin, R. C., Harrington, J. P., and Stecher, T. P. 1982, Ap. J., 252, 635.

Bruhweiler, F. C., Kondo, Y., and McCluskey, G. E. 1981, Ap. J. Suppl., 46, 255.

Caloi, V. 1972, Astr. and Ap., 20, 357.

Carnochan, D. J., and Wilson, R. 1983, Mon. Not. Royal Astr. Soc., 202, 317.

Drilling, J. S. 1983, Ap. J. (Letters), in press.

FitzGerald, M. P. 1968, Astr. J., 78, 983.

Greenstein, J. L. 1980, Highlights of Astronomy, 5, 255.

Greenstein, J. L., and Sargent, A. I. 1974, Ap. J. Suppl., 28, 157.

Hayes, D. S. 1979, Problems of Calibration of Multicolor Photometric Systems, ed. A. G. D. Philip (Dudley Obs. Reprint No. 14), p. 297.

Heber, U., Hunger, K., Jonas, G., and Kudritzki, R. P. 1983, preprint.

Hill, P. W., Kilkenny, D., Schönberner, D., and Walker, H. J. 1981, Mon. Not. Royal Astr. Soc., 197, 81.

Holmberg, E. B., Lauberts, A., Schuster, H.-E., and West, R. M. 1978, Astr. and Ap. Suppl., 31, 15.

Hunger, K., Gruschinske, J., Kudritzki, R. P., and Simon, K. P. 1981, Astr. and Ap., 95, 244.

Hunger, K., and Kudritzki, R. P. 1981, ESO Messenger, 24, 7.

Kaler, J. B., and Feibelman, W. A. 1983, preprint.

Kudritzki, R. P., and Simon, K. P. 1978, Astr. and Ap., 70, 653.

Kudritzki, R. P., Gruschinske, J., Hunger, K., and Simon, K. 1980, Proc. 2nd-year IUE-Conference, Tubingen.

Lucke, P. B. 1978, Astr. and Astr., 64, 367.

Michaud, G., Vauclair, G., and Vauclair, S. 1983, Ap. J., 267, 256.

Nandy, K., Thompson, G. I., Carnochan, D. J., and Wilson, R. 1978, Mon. Not. Royal Astron. Soc., 184, 733.

Paczynski, B. 1971, Acta. Astr., 21, 1.

Perry, C. L., and Johnston, L. 1982, Ap. J. Suppl., 50, 451.

Schönberner, D. 1979, Astr. and Ap., 79, 108.

Schönberner, D. 1981, Astr. and Ap., 103, 119.

Schönberner, D. 1983, Ap. J., in press.

Seaton, M. J., 1979, Mon. Not. Roy Astron. Soc., 187, 73P.

Sweigert, A. V., Mengel, J. G., and Demarque, P. 1974, Astr. and Ap., 30, 13.

Sweigert, A. V., and Gross, P. G. 1976, Ap. J. Suppl., 32, 387.

Walker, A. R. 1981, Mon. Not. Royal Astr. Soc., 197, 241.

Wesemael, F., Winget, D. E., and Cabot, W. 1982, Ap. J., 254, 221.

Winget, D. E., and Cabot, W. 1980, Ap. J. 242, 1166.

Table 1: Program stars and color excesses

Star	Images	E(B-V) (mag)	
LSS 1362	LWR 14242 SWP 18086	0.19	
LSS 2018	LWR 11405 SWP 14794	0.15	(0.18)
LSE 44	LWR 11409 SWP 14801	0.05	(0.11)
LSE 153	LWR 11406 SWP 14795	0.09	(0.09)
LSE 125	LWR 14243 SWP 18087	0.17	(0.21)
LSII-12^{o}1	LWR 11412 SWP 14812	0.25	(0.26)
LSE 259	LWR 14244 SWP 18089	0.20	
LSE 234	LWR 11407 SWP 14799	0.08	
LSE 263	LWR 13321 SWP 17051	0.11	
LSII 18^{o}9	LWR 11414 SWP 14821	0.05	(0.03)
LSE 21	LWR 13320 SWP 17050	0.18	(0.10)
LSIV 10^{o}9	LWR 11413 SWP 14813	0.07	(0.08)

Table 2: Hot stars with known effective temperatures

Star	T_{eff}	n(He)/n(H)	T_{BB}	R
HD 49798	47,500 (1)	1.0 (1)	58,000	2.30
BD $+75^{0}325$	55,000 (2)	1.5 (2)	63,000	2.52
HZ 43	55,000-70,000 (3)	$<10^{-3}$ (3)	89,000-105,000	3.04
NGC 7293	120,000 (4)	<0.1 (4)	170,000	3.89

1)Kudritzki and Simon, 1978.

2)Kudritzki, et al., 1980.

3)Auer and Shipman, 1977.

4)Bohlin, et al., 1982.

Table 3: Compositions and effective temperature of individual objects

Star	R	T_{BB}	T_{eff}		Surface Composition	T_{eff} (adopted)
			n(He)/n(H) =0.1	n(He)/n(H) = ∞		
LSS 1362	3.76	~ 170,000	-----	-----	normal or he-poor	~ 120,000
LSS 2018	3.03	110,000	85,000	105,000	normal	85,000
LSE 44	2.80	82,000	63,000	79,000	normal or he-poor	63,000
LSE 153	2.85	100,000	71,000	95,000	he-rich	89,000
LSE 125	3.18	125,000	95,000	117,000	normal	95,000
LSIV-12°1	2.89	90,000	69,000	87,000	normal	69,000
LSE 259	2.45	65,000	48,000	63,000	he-rich	59,000
LSE 234	2.63	100,000	71,000	95,000	normal	77,000
LSE 263	2.66	80,000	62,000	78,000	he-rich	74,000
LSII 18°9	2.66	77,000	60,000	74,000	normal or he-poor	60,000
LSE 21	3.92	~ 170,000	-----	-----	normal or he-poor	~ 120,000
LSIV 10°9	2.52	70,000	52,000	68,000	he-rich	65,000

Table 4: Distances and luminosities

Star	V	Lucke		Fitzgerald		Perrry & Johnston	Nandy et al.
		Fig. 3	Figs.4-6	Fig. 3	Figs.5-8		
	(mag)	(pc)	(pc)	(pc)	(pc)	(pc)	(pc)
LSS 1362	12.5	1000	1200	100->1000	>1000	---	>1000
LSS 2018	12.26	750	900	500-1000	<2000	---	1400
LSE 44	12.45	250	90	150	<500	---	150
LSE 153	11.35	450	200	200	<500	---	250
LSE 125	12.38	850	500	400-1000	>500	---	400
LSIV-12^{0}1	11.14	250	300	---	<500	---	600
LSE 259	12.6	650	450	600	<1000	---	450
LSE 234	12.4	300	200	300	<500	---	300
LSE 263	11.8	250	200	---	<500	---	300
LSSII 18^{0}9	12.13	100	150	<200	<500	80	150
LSE 21	11.78	600	120	50	<500	---	450
LSIV 10^{0}9	11.99	300	200	250	<500	250	150

Adopted Distance (pc)	M_V (mag)	Log L/L_o
~ 100	~ 6.9	~ 2.0
1000 ± 300	1.8 + 0.8 - 0.6	3.7 + 0.5 - 0.6
150 + 100 - 50	6.4 + 0.9 - 1.1	1.4 ± 0.6
250 ± 100	4.1 + 1.1	2.8 ± 0.6 - 0.8
600 + 300 - 200	2.9 ± 0.9	3.4 ± 0.6
400 ± 150	2.3 + 1.0 - 0.7	3.2 + 0.5 - 0.6
550 ± 100	3.3 ± 0.4	2.6 ± 0.5
250 ± 100	5.2 + 1.1 - 0.7	2.2 + 0.5 - 0.6
250 ± 100	4.5 + 1.1 - 0.7	2.5 + 0.5 - 0.6
100 + 50 - 30	7.0 + 1.5 - 0.9	1.1 + 0.6 - 0.8
~ 50	~ 7.7	~ 1.7
230 ± 100	5.0 + 1.2 - 0.8	2.0 + 0.6 - 0.7

FIGURE CAPTIONS

Fig. 1a,b Calibrated and dereddened IUE spectrograms of our O-type subdwarfs, arranged in the order of decreasing R.

Fig. 2: R vs. T_{BB} for the objects in Fig. 1 (filled circles), for standard stars with known temperature (crosses; see text), and for Planck's law (solid curve). Typical errors are also indicated. The measurements for LSE 21 and LSE 1362 are marked with arrows.

Fig. 3: Dereddened flux of LSE 2018 compared with two model atmospheres: 80,000 K and log g = 5 (solid curve); 100,000 K and log g = 6 (dashed curve), both with n(He)/n(H) = 0.1. A 10% error bar is shown in the upper left corner.

Fig. 4: H.R.-diagram in a (M_V, Log T_{eff})-representation with the central star region (CPN) to the left of the shaded line, the helium main sequence (from Pacyznski 1971), the extended horizontal branch (q), and the loci of our objects (squares). The evolutionary paths of post-AGB models of 0.565 and 0.644 M_0 are from Schönberner (1979, 1983), that of a 0.5 M_0 pure helium star from Paczynski (1971). The central helium burning phase of a EHB-model with M = 0.5 M_0 and q = 0.95 according to Sweigart and Gross (1976) is also shown. The (estimated) evolution of a 0.5 M_0 EHB-star with q = 0.98 is marked by a dashed line. The crosses indicate the termination of central

helium burning. The sdO's (circles) from Hunger et al. (1981) and sdB's (triangles) from Heber et al. (1983) are also displayed. The n(He)/n(H) ratios are indicated as follows: (open symbols normal or helium poor; half filled: helium rich; three quarter filled: probably extremely helium rich; filled: extremely helium rich). The arrow indicates the evolutionary direction of BD $+13^{o}3224$.

Author's Address: Department of Physics and Astronomy
Louisiana State University
Baton Rouge, Louisiana 70803-4001

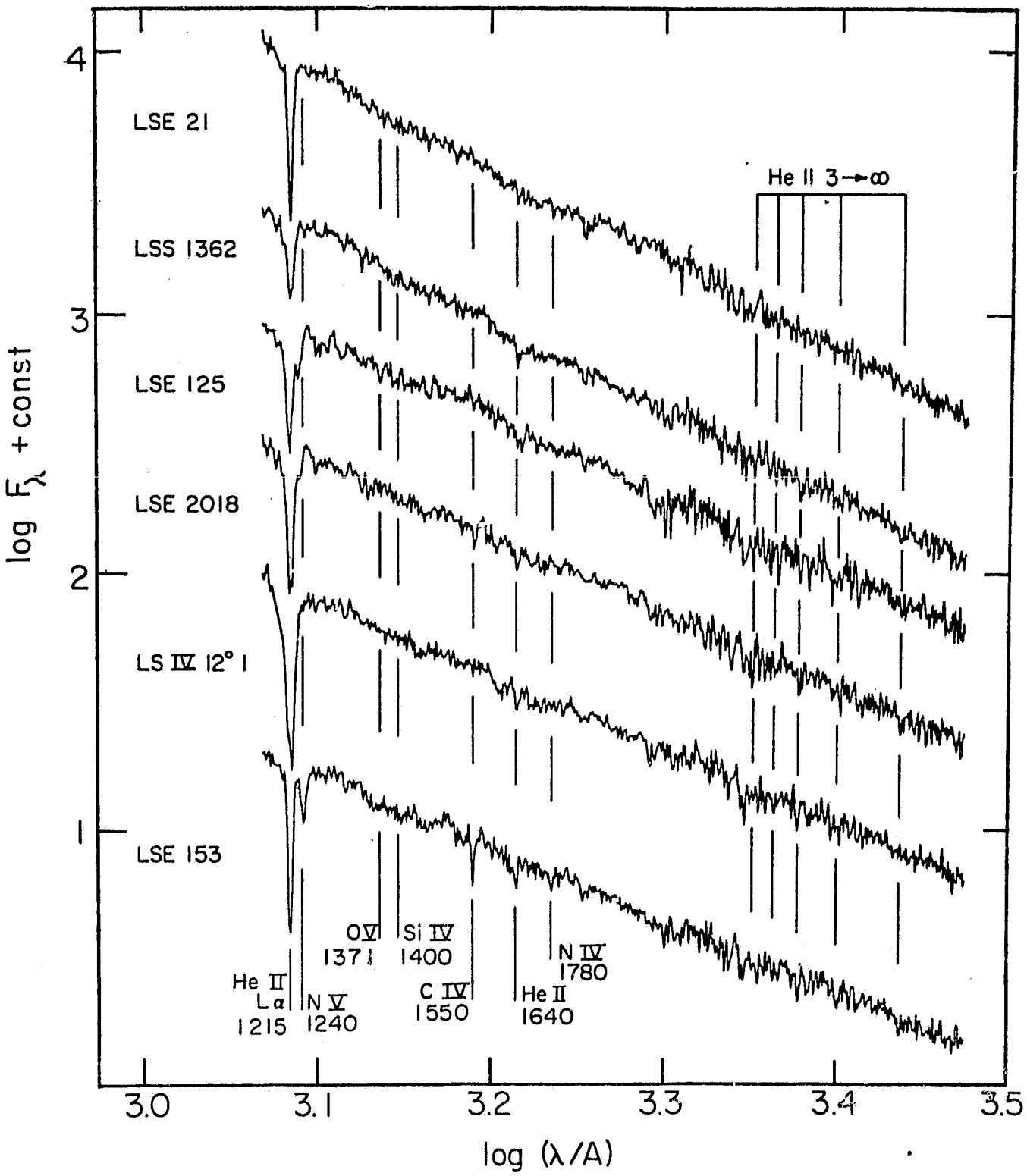

Schönberner & Drilling Fig 1a

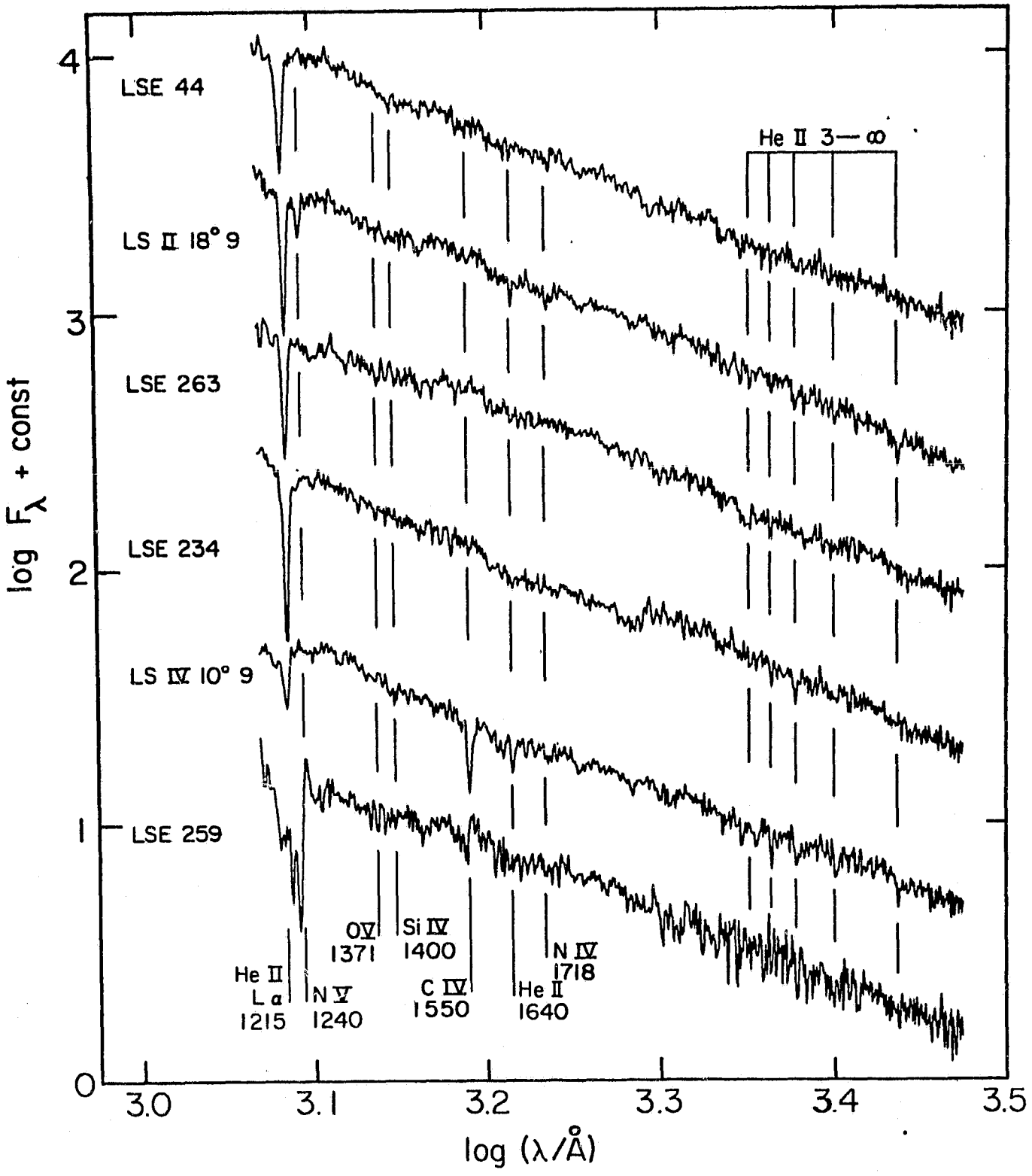

Schönberner & Drilling Fig 1b

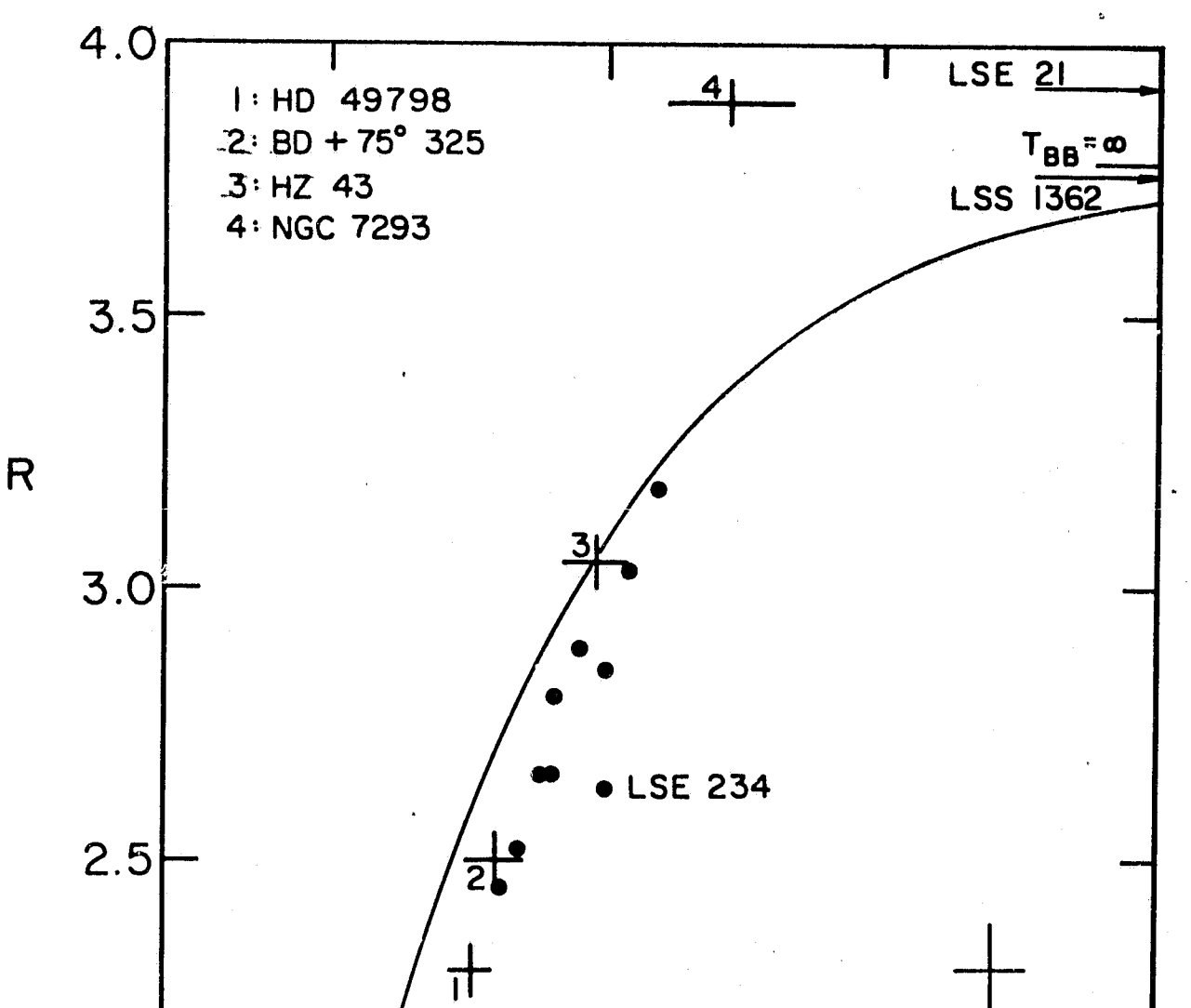

Schönberner & Drilling Fig. 2

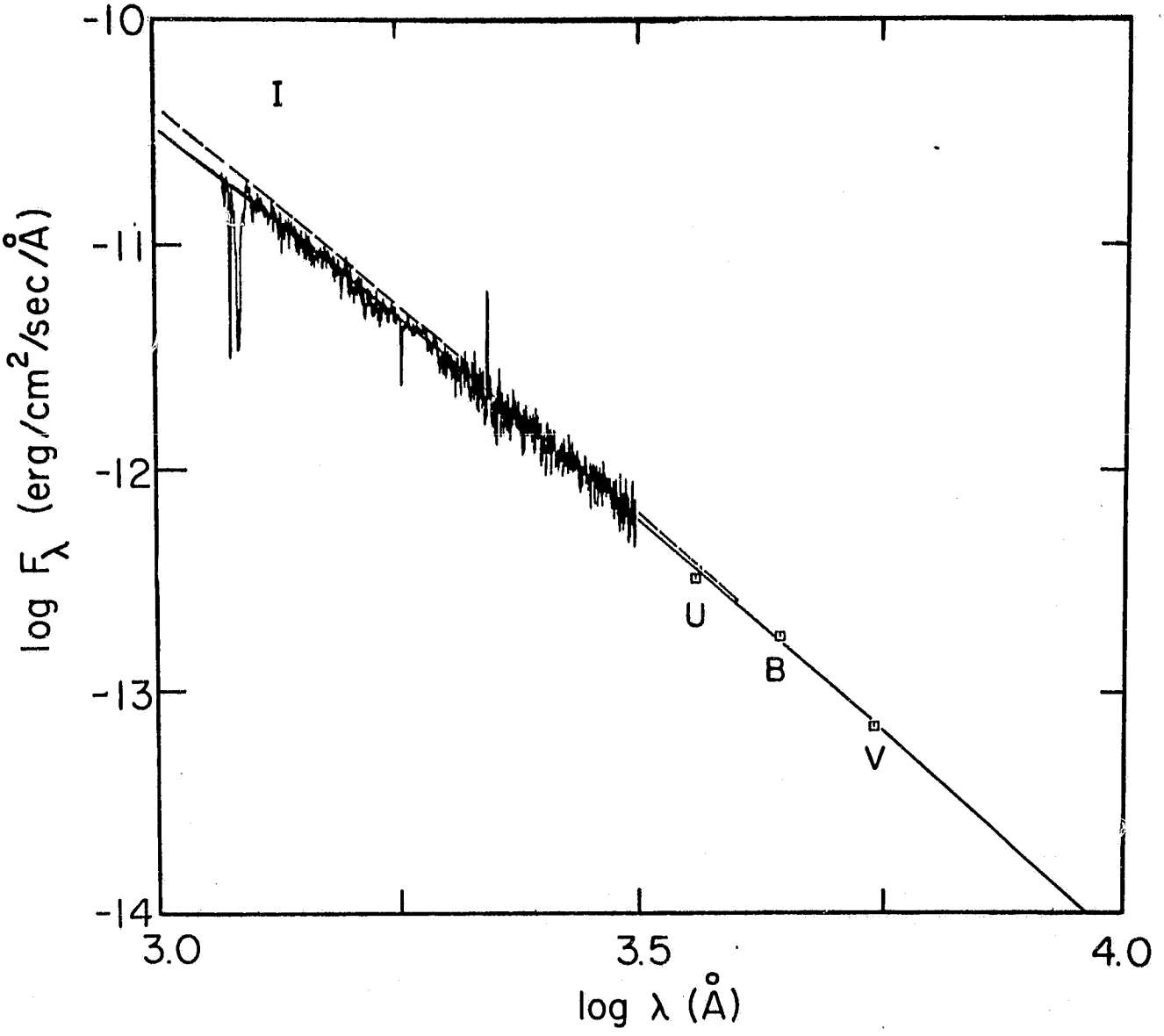

Schönberner & Drilling Fig. 3

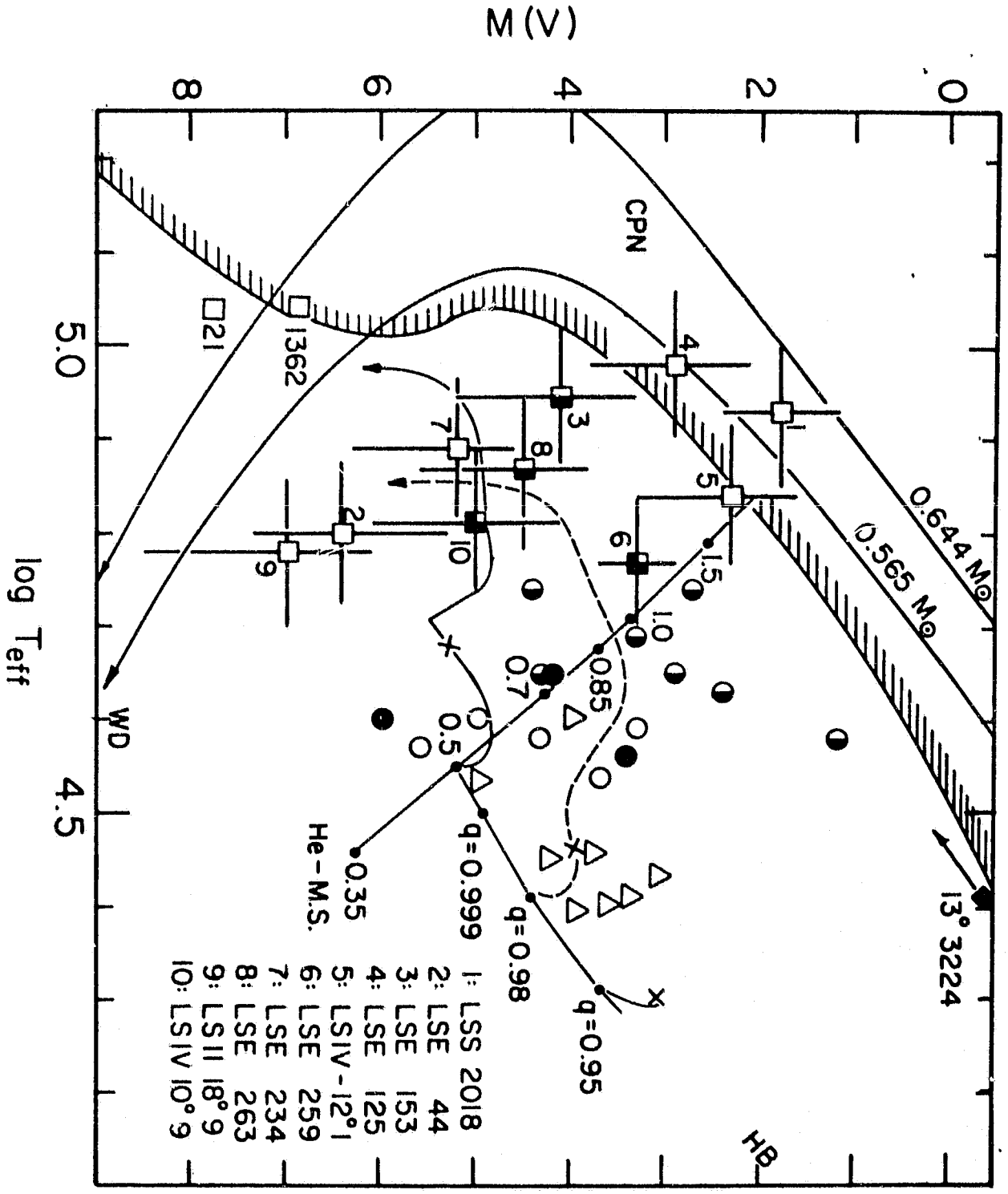

Schönberner & Drilling Fig. 4